Diffusion of cultural innovation depends on demography: testing an epidemiological model of cultural diffusion with a global dataset of rock art sites and climate-based estimates of ancient population densities

Authors: Richard Walker[*†1], Anders Eriksson[*†2], Camille Ruiz[3], Taylor Howard Newton[1], Francesco Casalegno[1]

Affiliations

[1] Blue Brain Project, Ecole Polytechnique Fédérale de Lausanne, Switzerland

[2] Department of Medical and Molecular Genetics, Kings College, London, UK

[3] Ateneo de Manila University, Manila, The Philippines

[†]Joint first authors

[*]Correspondence : richard.walker@epfl.ch, anders.eriksson@kcl.ac.uk

Abstract

Demographic models of human cultural evolution have high explanatory potential but weak empirical support. Here we use a global dataset of rock art sites and climate and genetics-based estimates of ancient population densities to test an epidemiological model, where the spread of an innovation requires population density beyond a critical value. We show that the model has stronger empirical support than a null model, where rock art detection rates and population density are independent, or a proportional model where detection is directly proportional to population density. Comparisons between results for different geographical areas and periods yield qualitatively similar results, supporting the robustness of the model. Re-analysis of the rock art data, using a second set independent population estimates, again yields similar results. We conclude that a minimum population density is a necessary condition for the spread of rock art. Methods similar to those described can be used to test our model for other classes of archaeological artifact and to compare the epidemiological model against other demographic models.

Introduction

It is widely accepted that the complexity and diversity of human cultures are a result of Cumulative Cultural Evolution (CCE), enabled by humans' unique neuroanatomy and cognitive capabilities, especially their skills in "cultural learning" [1–3] . However, the old idea that modern human capabilities emerged suddenly as a result of a highly advantageous mutation some 50,000 years ago [4,5] is no longer accepted and many allegedly modern features of human behavior and cognition are now believed to be more ancient than previously

suspected [6–9]. There is, furthermore, not the slightest evidence that variations in brain size, brain morphology or innate capabilities explain any aspect of the spatiotemporal patterning of human cultural evolution over the last 50,000 years. Against this background, demographic models of CCE [10] assign a determining role to variations in population size, density and structure. Such models suggest that larger, denser, better connected populations produce more innovations than smaller ones [11], are less vulnerable to stochastic loss of unique skills [12,13], and are more capable of exploiting beneficial transmission errors during social learning [14]. They also suggest that well-connected metapopulations produce faster cultural innovation than metapopulations with weaker connections among subpopulations [15] .

Demographic models could potentially provide valuable explanations for spatiotemporal patterning in the global archaeological record and several authors have used them for such purposes e.g. [14,16]. However, the assumptions and conclusions of the models are hotly contested [17–19]. Empirical studies are sparse and inconclusive, with some supporting an important role for demography e.g. [14,15,20,21], while others find no evidence for such a role [22–26].

In general, previous empirical studies have used data for historical or recently extinct hunter-gatherer populations from specific geographical regions. Here, for the first time, we test a demographic model of cultural evolution against fine-grained estimates of prehistoric population densities covering the whole globe, for a period of 46,000 years. Specifically, we test the ability of the model to predict the global, spatiotemporal distribution of parietal rock art sites over this period.

Results and discussion

An epidemiological model of cultural diffusion

CCE involves the inception, diffusion and selective retention of cultural innovations such as new behaviors and practices, new beliefs, and new technologies. In this study, we consider the case of parietal rock art. The model tested here (see Fig 1), inspired by SIR models in epidemiology [27–29], focuses on cultural diffusion [30], treated as analogous to the spread of a disease. The underlying assumption is that an innovation that does not spread beyond the population where it originates is unlikely to contribute to CCE or to leave a trace in the archaeological record.

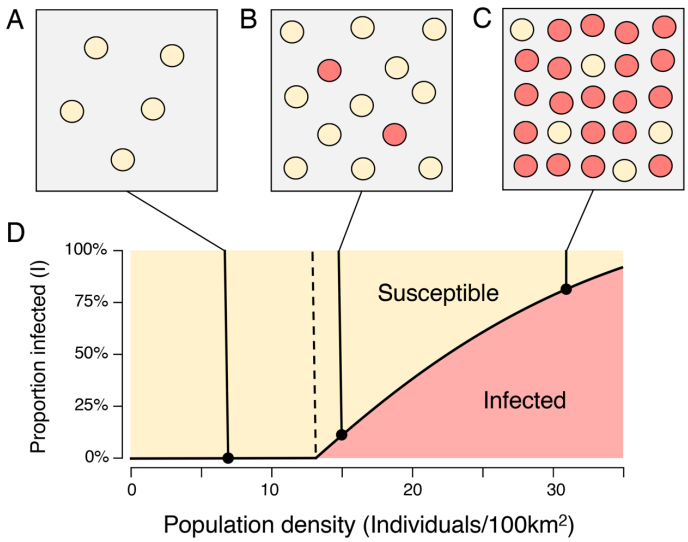

Fig 1. The epidemiological model. As population density increases, opportunities for transmission between subpopulations also increase. **A:** Below the critical threshold ρ^*, the innovation cannot spread between subpopulations. **B-C:** Above the critical threshold the proportion of infected subpopulations is an increasing function of population density.

Consider the emergence of rock art in a metapopulation comprising N subpopulations or communities, where I and S are respectively the proportion of *infected* communities (communities that have adopted the innovation), and *susceptible* communities (communities that have not). The innovation spreads from infected to susceptible communities at rate β. By analogy with empirical findings in [31] (see Methods), rates of encounter between communities are assumed proportional to the square root of population density. Infected communities *recover* (here: lose the ability to produce rock art) at rate γ.

In this model (see Fig 1 and Methods), there is a critical population density:

$$\rho^* = \left(\frac{\gamma}{\beta}\right)^2$$

such that

$$I^* = \begin{cases} 0, \rho \leq \rho^* \\ 1 - \sqrt{\frac{\rho^*}{\rho}}, \rho > \rho^* \end{cases}$$

The value of ρ^* is determined by the equilibrium between the rate of transmission, β , and the rate of recovery, γ. Below ρ^*, there are no infected communities; above ρ^*, I^* is an increasing function of population density. However, I^* is not directly observable in the archaeological record. To test our model, we therefore consider the *site detection rate* i.e. the small probability, P, that a territorial cell of defined area contains at least one recorded instance of rock art. Since the proportion of cells where geology, climate and research effort allow the creation, preservation and recording of rock art is small,

$$P \cong \zeta\, I^*\, \rho$$

where ζ reflects the joint effects of these factors (see SI). The model predicts that for $\rho \leq \rho^*$, detection rates will be zero and that at higher densities it will rise approximately in direct proportion to ρ. As a result, the shape of the distribution of sites by population density will differ significantly from the distribution of globals and median population density for cells containing sites will be automatically higher than for the complete set of cells.

Testing the model

Strategy

To test the predictions of the model, we collated a dataset containing the locations, dates and characteristics of 133 scientifically dated rock art sites (see Fig 2A, SI Table 1, Methods). Ancient population densities were estimated by combining data from two published models, informed by global genetic variation, and climate-based estimates of Net Primary Productivity [32,33] (See Methods). Population densities were inferred for all cells containing rock art site (*sites*) and for all cells (*globals*) (see Fig 2B). *Sites* and *globals* with inferred population densities of zero were eliminated from the subsequent analysis. We then computed site detection rates (number of sites / number of globals) as a function of population density for all latitudes between 20-60°N and 10-40°S, and all dates more recent than 46,000 years ago - the only latitudes and dates with significant numbers of sites in our sample. After exclusion of 4 sites at equatorial latitudes, 1 site older than 46,000 years and 8 sites with inferred population densities of zero, our final analysis included 119 *sites* and 9.8 million globals, with the age distribution shown in Fig 2C (see Methods).

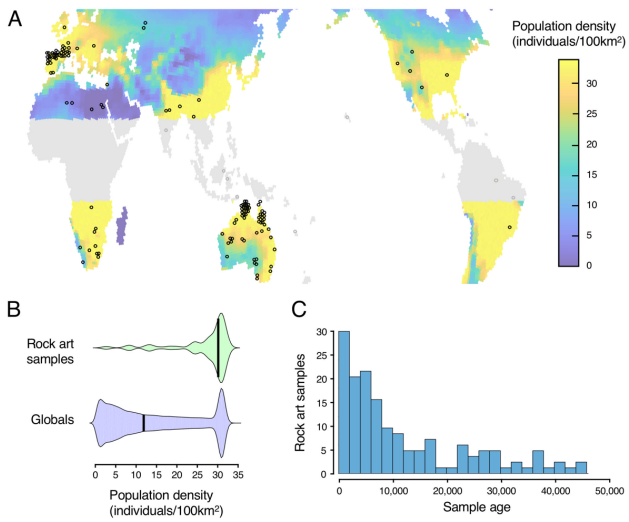

Fig 2. Sites used in the analysis: **A:** Geographical distribution of sites (all 133 sites) and inferred population distributions (maximum value over the last 46,000 years, see color bar for scale; areas excluded from the analysis shown in grey). **B:** comparison of population densities for all sites vs. all globals (119 sites included in analysis). **C:** distribution by earliest date of rock art at site location (119 sites included in analysis).

Empirical support for the model

Full dataset

As a first test of the model, we analyzed population densities for our complete rock art dataset. As predicted, the distribution of population densities for sites differed significantly from the

distribution for globals (two sample KS test D=0.55, p<0.0001), the proportion of sites in cells with low population densities was much lower than the proportion of globals , and the proportion in cells with high densities was much higher (median population densities: Sites: 29.92/100km^2; Globals 15.31/100km^2, Mann-Whitney U=305, p<0.01) (See Table 1 for detailed results).

Using a Bayesian statistical framework, we estimated the most plausible parameter values for the epidemiological model given the empirical observations (Fig 3A). Posterior distributions for model parameters were tightly constrained (see SI Fig 1). The inferred critical population density for the model with the highest likelihood, was 13.18 individuals/100km^2 (95% CI: 6.66 -17.00). Comparison of the epidemiological model against a constant model (equal site frequency at all population densities) strongly supported rejection of the alternative model. Comparison against a proportional model, where detection rates were directly proportional to population density (i.e. to the number of potential inventors in the population) (compare with [11]), again supported the superiority of the epidemiological model. (for detailed results see Table 1). Taken together, these findings strongly support the notion that the emergence of rock art requires population density above a critical value.

Analysis	Eriksson	Eriksson exact direct	Timmermann	Australia	France-Spain	0 - 9,999 years ago	10,000 - 46,000 years ago
N sites	119	55	97	56	31	74	45
N. Globals	9769332	9769332	213207	1223500	240461	2672852	7096480
Median population density Sites	29.92	30.25	25.02	30.25	28.23	30.36	27.19
Median population density Globals	15.31	15.31	18.04	21.50	26.60	19.92	13.66
Kolmogorov-Smirnov D	0.55	0.61	0.57	0.64	0.68	0.76	0.52
Kolmogorov-Smirnov p	0.000053	0.000004	0.000102	0.000001	0.000000	0.000000	0.000165
Mann-Whitney U	305.00	242.00	243.00	245.00	260.00	203.00	384.00
Mann-Whitney p	0.001041	0.000042	0.007397	0.000048	0.000790	0.000005	0.019182
Threshold CI 0.025	6.67	7.95	13.80	13.22	0.11	9.41	1.07
Threshold CI 0.25	11.16	11.69	16.73	19.22	6.31	13.63	4.26
Threshold CI 0.5	13.18	14.50	18.50	27.08	14.10	15.51	5.87
Threshold CI 0.75	14.80	15.98	20.36	28.07	18.52	16.89	7.74
Threshold CI 0.975	17.00	17.89	22.15	28.99	32.73	18.93	14.14
Log Likelihood	-1403	-679	-823	-592	-303	-819	-559
Bayes Factor (w.r.t. proportional model)	1.62E+05	2.23E+05	4.33E+06	2.64E+04	1.93E+01	7.91E+03	8.00E+01
Bayes Factor (w.r.t. Constant model)	2.00E+27	3.43E+17	7.60E+08	1.67E+10	2.44E+02	4.74E+13	4.95E+10

Table 1: Summary of statistical results for the analyses described in the text: The Kolmogorov-Smirnov test tests the null hypothesis that the distribution of *sites* is not significantly different from the distribution of *globals.* The Mann-Whitney test (which is less sensitive) tests whether the medians of the distributions are the same. Threshold CIs show the inferred Confidence Intervals for the threshold, given the empirical data. Log Likelihood shows the Log Likelihood of the model, given the empirical data. The two Bayes factors shows the ratio of the marginal likelihood of the epidemiological model to the marginal likelihood of alternative models (see Methods).

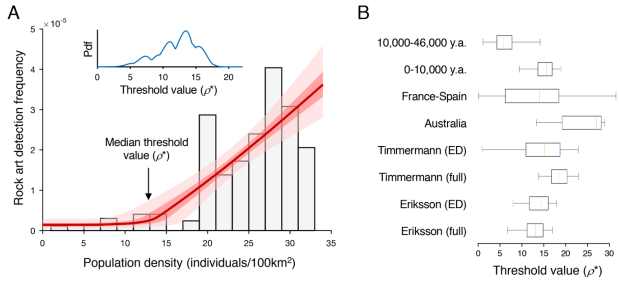

Fig 3. Empirical support for the epidemiological model. A. Inferred detection frequencies given the epidemiological model, the full archaeological dataset, and the combined population estimates from [32,33] (see Methods). Grey bars: Empirical frequencies of rock art in different intervals of population density. Red line: Estimated rock art detection rate as a function of population density (median of posterior distribution of estimated detection rate, with interquartile range in dark pink and 95% CI in pale pink). Also shown is the posterior probability density function (pdf) of the threshold value (ρ^*, inset); the median value of this distribution is indicated by an arrow on the main axis. B. Inferred values of the critical threshold for the different analyses described in the paper (ED: exact direct; orange line: maximum likelihood estimate; box: interquartile range; whiskers: CI 0.025-0.975).

Sites with exact dates obtained by direct methods

Seven sites in the rock art dataset were located in cells with estimated population densities below the critical value inferred from the model and the empirical data. As described in the Methods section, some of the dates in our rock art dataset were minimum or maximum dates, and some were estimated using indirect methods (e.g. dating of organic materials stratigraphically associated with the art). Since these dates do not necessarily reflect the actual dates at which the art appeared for the first time, and correct inference of population densities requires correct dates, we repeated our analysis using only sites with exact dates, obtained with direct methods. With this filtered dataset (55 sites), as in the original analysis, the distributions of population densities for sites and globals were significantly different (Two sample KS test D=0.61, p<0.00001**),** median population density for sites was higher than for globals (Sites: 30.25; Globals 15.31, Mann-Whitney U=242, p<0.0001) and, empirical support for the epidemiological model was much stronger than for alternative models (see Table 1). The inferred value of the critical population density (14.50 individuals/100km^2, 95% CI: 7.95-17.89) overlapped with the previous estimate (see Table 1).

Alternative population estimates

Another potential source of errors was the model used to generate our population estimates. We therefore repeated our analyses using more recent population estimates [34], based on a different climate model and different assumptions (see Methods). As in the earlier analysis, there were significant differences between the population density distributions for sites and globals, (two sample KS-test D=0.57, p<0.001), median inferred population was much higher for sites than for globals (sites: 25.02**;** globals: 18.04, Mann-Whitney U=243, p<0.01**)** and empirical support for the epidemiological model was much stronger than for the alternative null or proportional models (see Table 1). The CI for the inferred critical population density (95% CI: 13.80-22.15) overlapped with the CI for the original analysis (see Fig 3B, Table 1)

Potential sample bias

A comprehensive survey of the vast rock art literature was beyond the scope of our study. As a result, large geographical areas in Central/South America, Central Africa, East and South-East Asia are practically unrepresented in our dataset (see Fig 2A). Moreover, 60.9% of the sites in our full dataset date from less than 10,000 years ago, and only 3.8% from before 40,000 years ago (see Fig 2C). All this suggests the possibility of systematic bias. Suggestions that the literature itself is biased by ecological and taphonomic factors and by geographical variations in research effort [35] make the presence of such biases even more plausible.

To test the potential impact of such biases, we repeated our analysis for data from two culturally unrelated geographical areas (France-Spain and Australia) and for two distinct periods (from the present until 10,000 years ago, and from 10,000 until 46,000 years ago (see Methods). In the case of France-Spain, the predicted effects were attenuated by high estimated population densities even in areas with no sites. However, in all four cases, we found different density distributions for sites and globals, higher median population densities for sites than for globals, and stronger support for the epidemiological model than for alternative models (Table 1). Support for the existence of a critical population density for each of the periods and geographical areas examined is evidence that our results are not due to sampling biases (differences in sampling rates between periods or areas).

Population density as a proxy for social contacts

Another potential problem was the use of population density as a proxy for contacts between subpopulations. Grove suggests that individual encounter rates depend not on population density but on the product of density and mobility [31], and shows empirically that modern hunter gatherers' mobility is inversely proportional to the square root of population density. If this is correct, the encounter-rate will be directly proportional to the square root of population density. This is the assumption on which we based our model. However, testing with a generalized model (results not shown) demonstrated the robustness of our qualitative findings to the exact specification of this relationship (Methods).

Conclusions

This study models one of the key mechanisms required for CCE ("diffusion"), and tests the predictions of the model for the case of parietal rock art. In all our analyses, (Fig 3B, Table 1), the distribution of population densities for sites differs significantly than the distribution for globals and median population densities for sites (25-30 individuals/km^2) are consistently higher. In all cases, empirical support for the epidemiological model and a critical population density is much stronger than for alternative proportional or null models. Taken together, these results provide robust grounds to reject the null hypothesis that the emergence of rock art is unrelated to demography, and strong support for the epidemiological model i.e. for the notion that population density above a critical value is a *necessary* condition for its emergence.

Importantly, nothing in our model or empirical results suggests that a minimum level of population density is a *sufficient* condition for the emergence of rock art. There is little doubt, in fact, that, the creation, preservation and discovery of rock art depends on a multitude of factors, including variations in research effort as well as climatic and geological factors creating or limiting opportunities for its creation and preservation. It is not surprising, therefore, that many areas of the globe (e.g. in equatorial Africa) with high inferred population densities for the relevant periods, have little or no reported rock art. It is plausible, furthermore, that rock

art production depends not just on the population density of individual cells, but also on the overall size of so-called Culturally Effective Populations, spanning larger geographical areas, as posited by the demographic models reviewed in the Introduction. We consider the epidemiological model as complementary to these models.

The use of population density as the independent variable is, in fact, a key feature of our study: in archaeological contexts where a local population's cultural links to other populations are unknown, the size of "culturally effective populations" [12] is difficult to measure. A second key feature is the choice of "detection frequency" as the dependent variable: in the majority of current studies the dependent variable is "cultural complexity", usually quantified as the size of the population's toolkit [36]. The method used here circumvents the difficulty of applying such a concept in archaeological settings, where complete toolkits are rarely available. These methodological features of our study will facilitate the application of our model and methods outside the case of rock art and in contexts where other constructs are difficult to measure.

Our rock art dataset, population estimates, and software tools are publicly available at https://github.com/rwalker1501/cultural-epidemiology.git. Other researchers are encouraged to use them to replicate our findings, to test our hypotheses for other classes of artifact and with other population estimates, and to explore their own models.

Methods

Derivation of the model

The model describes the diffusion of a cultural innovation through a Culturally Effective Population (CEP) [12] i.e. a closed network of communicating individuals or subpopulations. Notation for the "disease dynamics" follows the conventions established in [29].

Consider a CEP with stable number of subpopulations, N. Assume that the population is divided into infected and susceptible (unaffected) subpopulations, with proportions I and S, respectively, such that $I + S = 1$. If the population is "well-mixed" (i.e. every subpopulation is in social contact with every other subpopulation), any infected subpopulation can transmit the innovation to any susceptible subpopulation. Let β be the rate of transmission per time step and γ the rate of recovery of the infected subpopulation (here: the rate at which it loses the ability to produce rock art). Thus, the rate of change in the proportion of infected subpopulations is given by

$$\frac{dI}{dt} = \beta \mathrm{NIS} - \gamma \mathrm{I} \tag{1}$$

In a partially connected population, infected subpopulations can only transmit an innovation to the susceptible subpopulations with which it is in contact. Assuming that on average each subpopulation is in contact with k other sub-populations, we can substitute k for N in Eq. (1). Using $S+I=1$, we thus obtain

$$\frac{dI}{dt} = \beta k I(1 - I) - \gamma I \tag{5}$$

Rearranging, solving for $\frac{dI}{dt} = 0$, and imposing $I^* \geq 0$, we obtain the stable proportion of infected subpopulations:

$$I^* = \begin{cases} 0, \ 1 - \frac{\gamma}{k\beta} \leq 0 \\ \left(1 - \frac{\lambda}{k\beta}\right), 1 - \frac{\gamma}{k\beta} > 0 \end{cases} \tag{6}$$

If social contact numbers k are proportional to the square root of density [31], i.e. k=$\alpha\sqrt{\rho}$,

$$I^* = \begin{cases} 0, 1 - \frac{\gamma}{\alpha\beta\sqrt{\rho}} \leq 0 \\ 1 - \frac{\gamma}{\alpha\beta\sqrt{\rho}}, 1 - \frac{\gamma}{\alpha\beta\sqrt{\rho}} > 0 \end{cases} \quad (7)$$

In short, there exists a critical population density, ρ^*, such that at densities below ρ^* there are no infected subpopulations, and at densities above ρ^*, the number of infected individuals is greater than zero.

At ρ^*, $1 - \frac{\gamma}{\alpha\beta\sqrt{p}} = 0$. Thus:

$$\rho^* = \left(\frac{\gamma}{\alpha\beta}\right)^2 \quad (8)$$

To reduce the number of parameters in the model, we normalize the rate of transmission, setting $\alpha\beta$ to 1. We thus obtain the simplified expressions:

$$\rho^* = \gamma^2 \quad (9)$$

and

$$I^* = \begin{cases} 0, \rho \leq \rho^* \\ 1 - \sqrt{\frac{\rho^*}{\rho}}, \rho > \rho^* \end{cases} \quad (10)$$

In this simplified version of the model, the equilibrium size of the infected population and the critical value of ρ are entirely dependent on population density and a single parameter, γ.

Finally, we assume that each infected subpopulation has an equal probability, z, of producing an artifact that produces a trace in the archaeological record. On this assumption, the probability *P,* that the n infected subpopulations will generate at least one such trace, is given by:

$$P = (1-(1 - zI^*)^N) \quad (11)$$

Assuming z is small, we obtain

$$P \cong zI^*N \quad (12)$$

The value of N for a cell of standard area, with fixed mean community size, is proportional to the population density for the cell:

$$N = \mu\rho \quad (13)$$

Grouping μ and z in a single variable ζ we obtain

$$P \cong \zeta\, I^*\rho \quad (14)$$

In the setting of our empirical study, inferred population sizes may contain large errors, especially when sites dates are minimum dates or indirect estimates. We, therefore, include an error term ε, representing the probability that a site is attributed to a cell with an incorrect date, whose population will thus be different from that of the cell with the correct date. Thus:

$$P = (1 - \varepsilon)\zeta I^*\rho + \varepsilon \quad (15)$$

This is the model we tested in our empirical study.

Rock art dataset

The analysis presented here is based on a dataset of parietal rock art, generated through a literature search with Google Scholar. We are aware that the database contains only a small proportion of all rock painting sites in the world, and that it may be subject to systematic biases. These are discussed in the Results and Discussion.

For the purposes of our survey, parietal rock art was defined to include all figurative and non-figurative pictograms (paintings and drawings) and petroglyphs (engravings) using rock wall as a canvas. “Art mobilier” (e.g. figurines) and geoglyphs (i.e. large designs or motifs on the ground) were excluded from the analysis.

The survey was seeded using the query:

("rock art" OR "parietal art" OR petroglyphs OR pictographs) [AND] (radiocarbon OR AMS OR luminescence OR Uranium).

We read the top 300 articles found by the query that were accessible through the EPFL online library, together with other relevant papers, cited within these articles. Sites where drawings, paintings and engravings were reported, were systematically recorded. Sites with no radiocarbon, optical luminescence or Uranium-Thorium date were excluded.

For each dated site, we recorded the longitude and latitude of the site (where reported), its name, the earliest and latest dates of “art” found at the site (converted to years before 1950 or years BP), the name of the modern country where the site was located, the journal reference, the method(s) used to produce the date, the nature of the dating procedure (direct dating, indirect dating), the nature of the data provided (exact data, minimum date, maximum date, mixed) a descriptor of the artefacts found (paintings, drawings, petroglyphs etc.), and a flag showing disputed dates. Where different authors reported different dates for a site, without disputing dates proposed by other authors, we systematically used the dates from the most recent report.

In cases where the article did not provide a latitude and longitude, online resources were used to locate the information. The main such resources were D. Zwiefelhofer’s FindLatitudeAndLongitude web site [37], which is based on Google Maps, and Austarch, a database of 14C and Luminescence Ages from Archaeological Sites in Australia, managed by A. Williams and Sean Ulm [38] .

The survey generated 190 records. Records with identical latitudes and longitudes and overlapping dates were merged (5 records eliminated). Duplicate records (12), modern sites (1), sites which did not meet the inclusion criteria (13), sites where the source was deemed unreliable (5), sites where reliable geographical coordinates were unavailable (12), sites with disputed or doubtful dates (8) and 1 site described in a retracted article were excluded. These procedures left a total of 133 records.

All except 5 of these records referred to sites located between 20°- 60°N and 10° - 40°S and with dates more recent than 46,000 years ago. Since the data analysis (see below) compares the distribution of population densities for *sites* against the distribution of *globals* defined as all cells, within a comparable range of latitudes, inclusion of these sites would have required the inclusion of an unrepresentative set of globals, potentially distorting the results of the analysis. They were therefore excluded from the subsequent analysis. For similar reasons, one

very early site (Blombos Cave, South Africa) (77,000 years ago) was also excluded. After these exclusions the dataset comprised 127 records. Subsequent analysis (see below) showed that 8 records referred to sites with estimated population densities less than 1 individual / 100km^2 at the date corresponding to the earliest rock art at the site. These sites were also excluded from the later phases of the analysis. Thus, the analysis was based on a final dataset of 119 records.

Estimates of population density

The population density estimates used in our paper combine results from a climate-informed spatial genetic model [32] with an improved model reported in [33]. Briefly, models combine climate estimates for the last 120,000 years, based on the Hadley Centre model HadCM3, with data on patterns of modern genetic variability from the human genome diversity panel-Centre d'Etude du Polymorphisme Humain (HGDP-CEPH), and a mathematical model of local population expansion and dispersal. Estimates of past precipitation and temperature are used to estimate Net Primary Productivity (NPP), and hence maximum human carrying capacity, for each cell in a hexagonal lattice with equal area cells 100 km wide, for all dates from 120,000 years ago to the present using time steps of 25 years. The carrying capacity is a continuous function of NPP governed by two NPP threshold values and a maximum carrying capacity parameter, K. The carrying capacity is zero below the lower NPP threshold, increases linearly from zero to K between the two NPP thresholds, and is constant and equal to K for NPP above the upper NPP threshold value. Human expansion out of Africa is simulated using a model where populations that have reached the maximum carrying capacity of a cell expand into neighboring cells. Approximate Bayesian Computing is used to compare models with a broad range of parameter values and starting values. Model evaluation is based on their ability to predict regional estimates of pairwise time to most recent common ancestor (TRMCA). We generated population size estimates using parameters from the high-ranking scenario described in Fig 2 and Movie S1 in [32] and NPP values from [33]. These contain a more accurate model of the American ice sheet dynamics and therefore give more accurate estimates of the colonization of the Americas by humans.

These population estimates were compared against the results using a second set of population estimates reported in [34]. The data refer to the early exit scenario (Scenario A) described in the paper. As in [32], human population density estimates are based on a climate model (LOVECLIM) combined with a reaction-diffusion Human Dispersal Model. Unlike the model in [32], the estimates do not take account of genetic data. A second difference concerns the population estimator, which is based not just on NPP but also on temperature and predicted "desert faction" and incorporates *ad hoc* modeling hypotheses absent in the previous model. These include accelerated human dispersal along coastlines ("a coastal express") and a special Gaussian decay function, modeling the probability of island hopping as a function of distance. For clarity of presentation, population estimates from the two models are both expressed in terms of effective population/ 100km^2.

Data analysis

In many sites in our dataset, the rock art reported in the literature spanned a broad range of dates. For the purposes of our analysis, we considered only the *oldest* date for each site. This procedure reduced our sample size and the statistical power of our analysis, but also the risk of artifacts due to dependencies in the data. Where confidence intervals were given, we used the midpoint of the interval. Each site was associated with the estimated population density for the

cell in the population model whose date and center point were closest to the date and location of the site. Globals were defined according to the needs of the individual analysis.

Analysis	Definition of globals
World	All cells with non-zero population with dates in the range 0-46,000 years ago and locations between 60°N and 20°N or between 10°S and 40°S
Periods	(1) All cells with non-zero population with age between 0 and 9,999 years. (2) All cells with non-zero population with age between 10,000 and 46,000 years.
France and Spain	Derived from the maximum and minimum latitudes and longitudes for sites in our dataset with locations in modern France or Spain. All cells with non-zero population lying in a "rectangle" with NW corner (lat: 50.84°N, lon: 10°) and SE corner (lat: 35.00°N, lon: 7.00°E)
Australia	Derived from the maximum and minimum latitudes and longitudes for sites in our dataset with locations in modern Australia. All cells with non-zero population lying in a "rectangle" with NW corner (lat: 25.27°S, lon: 133.77°E) and SE corner (lat: 39.16°S, lon: 154.86E)

Table 2: Definition of globals used in the different analyses Data for sites and globals were binned by population density (300 bins). Numbers of sites and globals and frequency of sites (sites/globals) were computed for each bin.

Testing model predictions

To test the predictions of the model for a specific dataset, we compared the distribution of sites by population density against the distribution of globals. Using the two-sided, two sample Kolmogorov-Smirnov test, we tested the null hypothesis that both were drawn from the same distribution, The difference between the medians of the two distributions was tested using the less sensitive Mann-Whitney U test.

Empirical support for the model was estimated using a Bayesian framework. For each of the parameters (γ, ζ and ε) we defined a uniformly distributed set of possible values lying within a plausible range and computed the likelihood of the model for all possible combination of these values, verifying the choice of parameter values using the computed posterior distributions. The value of the critical population density, ρ^* was inferred inserting the most likely inferred values of γ in the model

$$\rho^* = \gamma^2 \tag{15}$$

The most likely model was then compared against the most likely constant model, $z(\rho) = k$, and the most likely proportional model, $z(\rho) = \zeta\rho$. The relative likelihoods of the model were quantified using Bayes factors. The results are included in Table 1.

Analysis by period and geographical area

Subsets of "sites" and "globals" belonging to specific date bands (0 – 9,999 years ago, 10,000 – 46,000 years ago) and specific geographical areas with high numbers of sites (France/Spain, Australia) were subjected to the same analyses applied to the full dataset.

Sensitivity to the relationship between population density and encounter rate

To test the sensitivity of our model to the assumed inverse quadratic relationship between population density and encounter rate, we formulated a generalized version of our original model, where the critical population density and the encounter rates are power functions of population density. Thus:

$$\rho^* = \gamma^{\varphi}$$

$$I^* = \begin{cases} 0, \rho \leq \rho^* \\ 1 - \left(\frac{\rho^*}{\rho}\right)^{\frac{1}{\varphi}}, \rho > \rho^* \end{cases}$$

Replication of our analysis using this generalized model (results not shown) showed that our qualitative empirical findings are robust to the exact specification of the relationship between population density and encounter rate.

Software

Data extraction and analysis was based on custom code written in Python 2.7, using the Anaconda development environment.

Software availability

Python source code for the software used to perform the analyses is available under a GPL 3.0 license, at https://github.com/rwalker1501/cultural-epidemiology.git**.** The software includes (i) the script used to generate the figures and tables shown in this paper; (ii) methods to run additional data analyses and to produce figures not shown in the paper; (iii) a menu driven program providing easy to use access to these functions; (iv) documented source code for the statistical calculations and plots used in the paper and the additional analyses.

Data

The GIT repository includes the full rock art database used for the analysis, and copies of the population estimates from the Timmermann and the Eriksson models (reproduced with the permission of the authors). The original population estimates from Eriksson can be found at: https://osf.io/dafr2/ The original population estimates from Timmermann can be found at https://climatedata.ibs.re.kr/grav/data/human-dispersal-simulation.

References

1. Tomasello M. The cultural origins of human cognition. Harvard University Press; 2009.
2. Henrich J. The Secret of Our Success: How Culture Is Driving Human Evolution, Domesticating Our Species, and Making Us Smarter. Princeton University Press; 2015.
3. Laland KN. Darwin's unfinished symphony: how culture made the human mind. Princeton University Press; 2018.
4. Klein RG. Anatomy, behavior, and modern human origins. J World Prehistory. 1995;9: 167–198. doi:10.1007/BF02221838
5. Klein RG. Southern Africa and modern human origins. J Anthropol Res. 2001; 1–16.
6. McBrearty S, Brooks AS. The revolution that wasn't: a new interpretation of the origin of modern human behavior. J Hum Evol. 2000;39: 453–563.
7. d'Errico F, Stringer CB. Evolution, revolution or saltation scenario for the emergence of modern cultures? Philos Trans R Soc B Biol Sci. 2011;366: 1060–1069.
8. Scerri EM, Thomas MG, Manica A, Gunz P, Stock JT, Stringer C, et al. Did our species evolve in subdivided populations across Africa, and why does it matter? Trends Ecol Evol. 2018.
9. Galway-Witham J, Cole J, Stringer C. Aspects of human physical and behavioural evolution during the last 1 million years. J Quat Sci. 2019;34: 355–378.
10. Shennan S. Demography and Cultural Evolution. Emerging Trends in the Social and Behavioral Sciences. John Wiley & Sons, Inc.; 2015.
11. Kremer M. Population Growth and Technological Change: One Million B.C. to 1990. Q J Econ. 1993;108: 681–716. doi:10.2307/2118405
12. Shennan S. Demography and cultural innovation: a model and its implications for the emergence of modern human culture. Camb Archaeol J. 2001;11: 5–16.
13. Premo LS, Kuhn SL. Modeling effects of local extinctions on culture change and diversity in the Paleolithic. PLoS One. 2010;5: e15582.
14. Henrich J. Demography and cultural evolution: How adaptive cultural processes can produce maladaptive losses - The Tasmanian case. Am Antiq. 2004;69: 197–214. doi:10.2307/4128416
15. Powell A, Shennan S, Thomas MG. Late Pleistocene demography and the appearance of modern human behavior. Science. 2009;324: 1298–1301.
16. Lycett SJ, Norton CJ. A demographic model for palaeolithic technological evolution: the case of East Asia and the Movius Line. Quat Int. 2010;211: 55–65.
17. Collard M, Vaesen K, Cosgrove R, Roebroeks W. The empirical case against the 'demographic turn'in Palaeolithic archaeology. Phil Trans R Soc B. 2016;371: 20150242.
18. Vaesen K, Collard M, Cosgrove R, Roebroeks W. Population size does not explain past changes in cultural complexity. Proc Natl Acad Sci. 2016;113: E2241–E2247.
19. Henrich J, Boyd R, Derex M, Kline MA, Mesoudi A, Muthukrishna M, et al. Understanding cumulative cultural evolution. Proc Natl Acad Sci. 2016;113: E6724–E6725. doi:10.1073/pnas.1610005113
20. Kline MA, Boyd R. Population size predicts technological complexity in Oceania. Proc R Soc B Biol Sci. 2010; rspb20100452.
21. Collard M, Ruttle A, Buchanan B, O'Brien MJ. Population size and cultural evolution in nonindustrial food-producing societies. PloS One. 2013;8: e72628.
22. Collard M, Kemery M, Banks S. Causes of toolkit variation among hunter-gatherers: a test of four competing hypotheses. Can J Archaeol Can Archéologie. 2005; 1–19.

23. Collard M, Buchanan B, O'Brien MJ. Population size as an explanation for patterns in the Paleolithic archaeological record. Curr Anthropol. 2013;54: S388–S396.
24. Read D. An Interaction Model for Resource Implement Complexity Based on Risk and Number of Annual Moves. Am Antiq. 2008;73: 599–625. doi:10.2307/25470520
25. Read D. Population size does not predict artifact complexity: analysis of data from Tasmania, arctic hunter-gatherers, and Oceania fishing groups. UCLA Hum Complex Syst 2012. 2012 [cited 9 Feb 2016]. Available: http://papers.ssrn.com/sol3/papers.cfm?abstract_id=2460379
26. Buchanan B, O'Brien MJ, Collard M. Drivers of technological richness in prehistoric Texas: an archaeological test of the population size and environmental risk hypotheses. Archaeol Anthropol Sci. 2016;8: 625–634. doi:10.1007/s12520-015-0245-4
27. Ross R. An Application of the Theory of Probabilities to the Study of a priori Pathometry. Part I. Proc R Soc Math Phys Eng Sci. 1916;92: 204–230. doi:10.1098/rspa.1916.0007
28. Kermack WO, McKendrick AG. A contribution to the mathematical theory of epidemics. Proceedings of the Royal Society of London. The Royal Society; 1927. pp. 700–721. Available: http://rspa.royalsocietypublishing.org/content/royprsa/115/772/700.full.pdf
29. Hethcote HW. Three Basic Epidemiological Models. In: Levin SA, Hallam TG, Gross LJ, editors. Applied Mathematical Ecology. Berlin, Heidelberg: Springer Berlin Heidelberg; 1989. pp. 119–144. doi:10.1007/978-3-642-61317-3_5
30. Rogers EM. Diffusion of innovations. New York, NY: Free Press; 1962.
31. Grove M. Population density, mobility, and cultural transmission. J Archaeol Sci. 2016;74: 75–84.
32. Eriksson A, Betti L, Friend AD, Lycett SJ, Singarayer JS, Cramon-Taubadel N von, et al. Late Pleistocene climate change and the global expansion of anatomically modern humans. Proc Natl Acad Sci. 2012;109: 16089–16094. doi:10.1073/pnas.1209494109
33. Raghavan M, Steinrucken M, Harris K, Schiffels S, Rasmussen S, DeGiorgio M, et al. Genomic evidence for the Pleistocene and recent population history of Native Americans. Science. 2015;349: aab3884–aab3884. doi:10.1126/science.aab3884
34. Timmermann A, Friedrich T. Late Pleistocene climate drivers of early human migration. Nature. 2016;538: 92–95.
35. Bednarik RG. The pleistocene art of Asia. J World Prehistory. 1994;8: 351–375. doi:10.1007/BF02221090
36. Oswalt WH. An anthropological analysis of food-getting technology. New York, NY: Wiley; 1976.
37. Zwiefelhofer, D. FindLatitudeAndLongitude. [cited 12 Nov 2019]. Available: http://www.findlatitudeandlongitude.com/
38. Alan Williams, Sean Ulm. AustArch: A Database of 14C and Luminescence Ages from Archaeological Sites in Australia. In: Archaeology Data Service [Internet]. [cited 12 Nov 2019]. Available: https://archaeologydataservice.ac.uk/archives/view/austarch_na_2014/

Acknowledgements

The idea of testing our model on the case of parietal rock art emerged from a meeting at University College, London, between Richard Walker, Stephen Shennan & Mark Thomas (University College, London) and Anders Eriksson. Axel Timmermann, International Pacific Research Center, University of Hawaii kindly contributed population estimates. Michelle Langley, Griffith University, Brisbane, Australia; Australian National University, Canberra, Australia, contributed data from a published survey of Australian rock art. Werner van Geit, Blue Brain Project, EPFL, Switzerland, contributed important code fragments. Isabel Marquez cross-checked the data for rock art sites. Mark Thomas and Stephan Shennan, Michael Herzog (EPFL Switzerland), Ruedi Füschlin (ZHAW, Switzerland), Lenwood Heath (Virginia Tech, USA) and Francesco Walker (University of Enschede, the Netherlands) reviewed earlier versions of this manuscript, providing valuable feedback. Henry Markram, leader of the Blue Brain Project, provided vital encouragement and support.

Author contributions

RW developed the original epidemiological model and wrote a prototype version of the software.

AE contributed the population data used in the analysis, substantially contributed to the development of the epidemiological model, and developed the concepts and analysis tools used to validate the model. RW and AE jointly wrote the manuscript. CR rewrote the prototype data extraction and analysis software from RW and AE, and developed the publication version of the tool. TH contributed to the formal derivation of the epidemiological model. FC contributed to the statistical analysis.

Supplementary Information

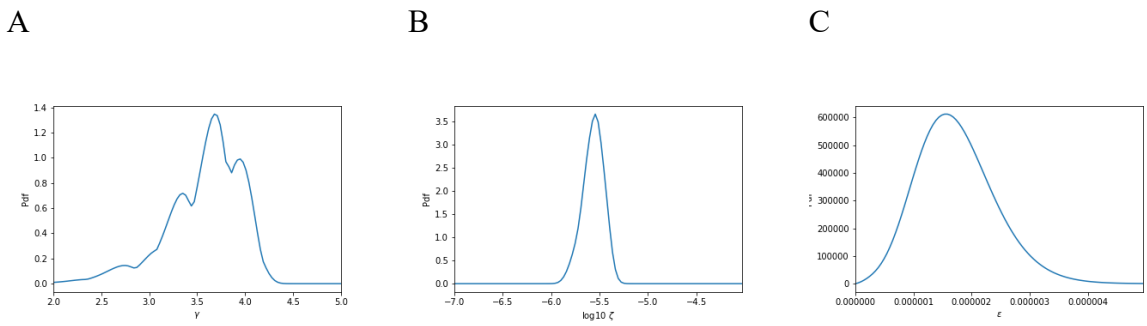

SI Fig 1: Posterior distributions for the γ, ξ, and ε parameters for the epidemiological model as shown in Fig 3A (observed site detection rates, for the full archaeological dataset and the combined population estimates in [28,29])

,

Supplementary Information Table 1: Rock art dataset (133 sites)

Name	Latitude	Longitude	Earliest age in sample	Latest age in sample	Modern Country	Date of reference	Dating method/comments	Direct / indirect	Exact Age / Minimum Age / Max Age	Calibrated	Kind	Figurative	Reference
Abri Castanet, Dordogne, France	44.999272	1.101261	37'205	36'385	France	2012	accelerator mass spectrometry (AMS), indirect (bone samples)	Indirect	Minimum Age	No	Petroglyphs	Yes	(1)
Altamira, Spain	43.377452	-4.122347	36'160	2'850	Spain	2013	Uranium-series dating	Direct	Exact Age	Unknown	Petroglyphs Decorated ceiling in cave	Yes, not all. One is linear red line.	(2)
Altxerri B, Spain	43.2369	-2.148555	39'479	34'689	Spain	2013	Indirect radiocarbon dating	Indirect	Minimum age	Yes	Painting	Yes	(3)
Anbarndarr I. Australia/Anbarndarr II, Australia/Gunbirdi I, Gunbirdi II, Gunbirdi III, Northern Territory Australia	-12.255207	133.645845	1'704	111	Australia	2010	Direct radiocarbon dating of beeswax sample	Direct	Exact age	Yes	Beeswax	No	(4)
Anta de Serramo, Vimianzo, A Coruña, Galicia, Spain	43.110048	-9.03242	6'950	6'950	Spain	2005	Direct radiocarbon dating, by AMS on charcoal	Direct	Exact age	Yes	Painting	N/A	(5)
Apollo 11 Cave, llKaras Region	-26.842964	17.290284	28'400	26'300	Namibia	1983	Radiocarbon dating	Indirect	Minimum age	Unknown	Painted fragments	Yes	(6)
ARN-0063, Namarrgon Lightning Man, Northern Territory, Australia	-12.865524	132.814001	1'021	145	Australia	2010	Direct radiocarbon from beeswax	Direct	Exact age	Yes	Beeswax	Yes	(4)
Bald Rock, Wellington Range,Northern Territory Australia	-11.8	133.15	386	174	Australia	2010	Direct radiocarbon from beeswax	Direct	Exact age	Yes	Beeswax	N/A	(4)
Baroalba Springs, Kakadu, Northern Territory, Australia	-12.677013	132.480901	7'876	7'876	Australia	2010	Indirect Carbon dating via minimum age of mineral salts from rock art surface sampled	Indirect	Minimum age	Yes	Painting	-	(4)
Bhimbetka, India	22.939546	77.612433	5'190	1'100	India	2005	Direct radiocarbon dating on white paint from figure	Direct	Exact Age	Unknown	Painting	Yes	(7)
Biggarsberg, South Africa	-26.286668	28.047223	4'050	970	South Africa	2003	Direct radiocarbon from oxalates underlying and overlying painting	Direct	Exact age	Unknown	Painting	N/A	(8)
Bighorn Basin, Wyoming and Montana, USA	44.379957	-108.038989	6'862	0	USA	1993	AMS Radiocarbon dating	Direct	Exact age	Yes	Petroglyphs	N/A	(9)
Billasurgam, Kurnool, Andra Panesh, India	15.828126	78.037279	5'620	4'825	India	2012	Radiocarbon dating of flowstone on top and below the engraving	Indirect	Minimum Age	Unknown	Petroglyph	No	(10)

Bindu, Kakadu, Northern Territory, Australia	-12.677013	132.480901	183	117	Australia	2010	Direct radiocarbon from beeswax	Direct	Exact age	Yes	Beeswax dots and lines	No	(4)
Bush Turkey Dreaming Site, Western Australia	-23.96	122.97	60	60	Australia	2010	Direct radiocarbon from beeswax	Direct	Exact age	Yes	Painting	Yes	(4)
Cape York, Australia	-10.7	142.516667	730	725	Australia	1993	Direct radiocarbon dating on plant-fibre binders	Direct	Exact age	Unknown	Painting	N/A	(11)
Casota do Paramo, A Coruña, Spain	42.704644	-8.930863	5'400	5'400	Spain	2005	Direct radiocarbon dating of charcoal paint samples	Direct	Maximum Age	Yes	Painting	No	(5)
Cave of Beasts, Gilf Kebir, Egypt	23.441389	25.839722	8'450	6'350	Egypt	2014	Radiocarbon dating, pottery typology	Indirect	N/A	Unknown	Painting	Yes	(12)
Cave of Bees, Matopos, Zimbabwe	-20.557222	28.5125	10'500	10'500	South Africa	1983	Radiocarbon dating on painted spall	Direct	Exact age	Unknown	Painting	N/A	(6)
Cave of Cougnac, France	44.756986	1.375957	24'000	24'000	France	2001	Direct Radiocarbon dating on charcoal from paintings	Direct	Exact Age	Unknown	Painting	Yes (2 deers)	(13)
Cave of El Castillo, Spain	43.292368	-3.965576	41'400	22'880	Spain	2012, 2001,	Uranium Series disequilibrium dates of calcite deposits overlying or underlying art	Direct	Minimum Age	Yes	Pike: Painting	Pike: Some, most are disk-shapes Valladas 2001: Yes Valladas 1992: Yes	(14)
Cave of Niaux, France	42.820098	1.593487	12'890	12'890	France	1992	Valladas 1992: Direct radiocarbon dating Clottes 1992:	Direct	Exact age	Unknown. Likely no	Painting	Yes	(15)
Chauvet-Pont-d'Arc Cave, France	44.387244	4.415865	32'410	30'340	France	2001	Direct radiocarbon dating from painting	Direct	Exact age	Unknown.	Painting	Yes	(16)
Chifubwa Stream Shelter, Zambia	-12.2	26.683333	6'300	6'300	Zambia	1979	Indirect radiocarbo	Indirect	Minimum age	No	Engraving	No	(17)
Coliboaia Cave, Romania	46.53089	22.597332	32'000	32'000	Romania	2012	Radiocarbon dating of charcoal layer atop drawing	Direct	Exact age	Unknown	Drawings	Yes	(18)
Cosquer cave, Calanque de Morgiou, France	43.210931	5.445896	28'370	17'800	France	2001	Radiocarbon dating	Direct	Exact Age	No	Painting	Yes	(16)
Coto dos Muros, Baixo Miño, Northwest Iberia	41.999517	-8.770147	6'340	4'020	Spain	2005	Radiocarbon dating	Direct	Maximum Age	Yes	Painting	N/A	(5)
Covaciella, Spain	43.318232	-4.875262	17113	16'881	Spain	2001	Radiocarbon dating	Yes	Exact age	Yes	Painting	Yes	(16)
Deighton Lady, Jowalbinna, Queensland Australia	-15.5333	144.7833	6'483	2'905	Australia	2010	Minimum age radiocarbon dating based on minimum age of oxalate sample	Indirect	Minimum age	Yes	Engraving	No	(4)
Djarrng, West Arnhem Land, Northern Territory, Australia	-12.091834	132.890495	720	119	Australia	2010	Direct radiocarbon from beeswax	Direct	Exact age	Yes	Beeswax	Yes	(4)

Djulirri, Arnhem Land, Northerm Territory, Australia	-12.091834	132.890495	383	172	Australia	2010	Direct radiocarbon from beeswax	Direct	Exact age	Yes	Beeswax	Yes	(4)
East Alligator River, Northern Territory, Australia	-12.525429	133.060161	4'287	122	Australia	2010	Direct radiocarbon from beeswax	Direct	Exact age	Yes	Beeswax	No	(4)
Echidna's Rest, Queensland, Australia	-27.542345	153.07315	1'291	Modern	Australia	2010	Direct radiocarbon from charcoal	Direct	Exact age	Yes	Drawings and engraving	No	(4)
El Hosh, Egypt (6km north of Gebel Silsila)	24.642614	32.92968	7'550	2'325	Egypt	2001	Direct radiocarbon dating	Direct	Exact Age	Yes	Petroglyphs	Yes	(19)
Emu Cave, New South Wales, Australia	-33.782342	150.590426	1'857	1'857	Australia	2010	Radiocarboon dating on sample collected from over an emu track	Indirect	Minimum age	Yes	Engraving	Yes	(4)
Fariseu, Coa Valley, Portugal	41.079991	-7.111782	18'400	10'800	Portugal	2006	optical luminescence (OSL) from burnt lithic remains	Indirect	Minimum age	No	Petroglyphs	Yes	(20)
Fetra Hé Cave, Lifou Island, New Caledonia	-21.038497	167.240515	2'570	983	New Caledonia	2006	Radiocarbon dating	Direct	Exact age	Yes	Hand stencils	Some	(21)
Forno dos muros, portugal	40.224238	-8.636221	5'840	5'505	Portugal	2005	Direct radiocarbon	Direct	Exact age	Yes	Painting	N/A	(5)
Foz Coa, Portugal	41.082247	-7.14036	2'000	100	Portugal	1996	Radiocarbon dating of microorganisms in cracks in engravings	Indirect	Minimum age	No	Petroglyphs	Yes	(22)
Fuente de el Salin, Muñorrodero Spain	43.364429	-4.482981	22'340	22'340	Spain	2017	Indirect radiocarbon dating on charcoal from associated hearth	Indirect	Minimum age	Unknown	Painting	N/A	(23)
Gargas, France	43.90322	5.357388	26'860	26'860	France	1992	Radiocarbon dating	Indirect	Minimum age	Unknown	Hand stencils, engravings	Yes	(24)
Giant Horse, Laura, Queensland, Australia	-15.5384	144.4566	474	474	Australia	2010	Direct radiocarbon in layered paint	Direct	Exact age	Yes	Painting	-	(4)
Glen Canyon, South-central Utah, USA	37.386989	-110.842823	1'080	675	USA	1992	Radiocarbon dating of associated artifacts	Indirect	N/A	Unknown	Painting	Yes	(25)
Grande Grotte, Arcy-sur-Cure, France	47.591452	3.766392	45'504	29'173	France	2013	Indirect radiocarbon dating on associated bone and tooth specimens	Indirect	N/A	Yes	Painting	N/A	(26)
Grotta di Fumane, Italy	45.592481	10.90443	41'000	41'000	Italy	2009	Radiocarbon dating of wood carbon associated with paintings	Indirect	Exact Age	Yes	Painting	Yes	(27)
Grotte d'Aldène, Cesseras, France	43.353897	2.698387	30'260	30'260	France	2005	AMS	Indirect	N/A	Unknown	Engravings	N/A	(28)

Grotte de Cussac, Dordogne River Valley, France	44.829444	0.847778	29'209	3'426	France	2017	U eTh and 14C for speleothems, 14C-AMS for organic materials, bone and charcoal	Indirect	Mixed	Unknown	Painting	Yes	(29)
Gua Saleh, Sangkuliran - Mangkalihat Peninsula, Kalimantan Island, Indonesia	1.035717	118.065445	27'270	9'820	Indonesia	2003	Cross-dating using Th/U and AMS of calcite covering paintings	Indirect	Minimum age	Yes	Paintings	Yes	(30)
Gunbilngmurrung, Australia	-12.8	133.3	3'870	140	Australia	2010	Direct radiocarbon on beeswax	Direct	Exact Age	Yes	Beeswax	Yes	(31)
Hathitol, India	23.152243	79.920672	4'810	2'780	India	2005	DIrect radiocarbon on painting pigment	Direct	Exact Age	Unknown	Painting	Yes	(7)
Hay Cave, Queensland, Australia	-23.167328	150.490387	2'420	1'010	Australia	2010	Direct charcoal pigr	Direct	Exact age	No	Painting	No	(4)
Ignatievskaya Cave, Russia	54.899497	57.781586	8790	6925	Russia	2002	Radiocarbon dating on charcoal pigment	Direct	Exact Age	Unknown	Painting	Yes	(32)
Ingaladdi, willeroo, Northern Territory, Australia	-15.29028	131.575195	7'676	7'676	Australia	2010	Radiocarbon dating on charcoal sampled using minimum age	Indirect	Minimum age	Yes	Engraving	N/A	(4)
Jamjori, India	24.515475	87.081156	1'720	1'720	India	2005	Direct radiocarbon dating on paint	Direct	Exact Age	Unknown	Painting	No	(7)
Jinsha, China	26.855047	100.22775	5'216	5'216	China	2012	Uranium-series dating on calcite samples above and beneath painting	Indirect	Maximum Age	N/A	Painting	Yes	(33)
Kaalpi site, Western Australia (Near Calvert Ranges)	-23.95	122.72	377	308	Australia	2010	Radiocarbon dating of sample pigment	Direct	Exact age	Yes	Painting	N/A	(4)
Kaho'olawe, Hawai'i, USA	20.558047	-156.605738	923	0	Hawaii	1996	Radiocarbon dating of sampled petroglyph	Indirect	Minimum age	Yes	Painting	Yes	(34)
Kapova cave, Russia	53.043799	57.065139	14'680	13'930	Russia	1989	Radiocarbon dating of charcoal from cultural stratum	Indirect	Unknown	Unknown	Painting	Yes	(35).
Kennedy River, Queensland, Australia	-15.5906	144.0308	1'132	1'132	Australia	2010	Radiocarbon dating of oxalate sample	Indirect	Minimum age	Yes	Engraving	Yes	(4)
Kimberley, Australia	-17.34918	125.915207	4'300	1'350	Australia	2010	Radiocarbon dating of paint	Direct	Exact age	Yes	Painting	Yes	(4)
La Garma, Cantabria, Spain	43.151944	-3.896389	16'875	16'875	Spain	2013	Direct radiocarbon dating	Direct	Exact age	Yes	Paintings	Yes	(26)
La Pileta, Spain	36.691297	-5.2699	24'228	24'228	Spain	2013	Direct radiocarbon dating	Direct	Exact age	Yes	Paintings	Yes	(26)
La Tête du lion, France	45.777403	4.855214	26'760	25'997	France	2013	Indirect radiocarbon dating on charcoal	Indirect	Minimum age	Yes	Paintings	N/A	(26)

Labastide, France	43.035546	0.352267	17'476	484	France	2013	Radiocarbon dating	Direct	Exact age	Yes	Paintings	Yes	(26)
Lapa do Santo, Brazil	-19.477778	-44.038889	10'600	10'600	Brazil	2012	Direct radiocarbon ages assisted by OSL	Yes	Exact age	Yes	Petroglyph	Yes	(36)
Lascaux Cave, France	45.053919	1.167651	22'723	18'848	France	2013	Radiocarbon dating	Indirect	Minimum age	Yes	Paintings	Yes	(26)
Lene Hara Cave, East Timor	-8.411695	127.293235	11'350	11'350	East Timor	2007	Plasma mass spectrometry	Direct	Exact age	Yes	Paintings	N/A	(37)
Lower Pecos, Texas	31.422912	-103.493229	3'865	3'865	USA	1995	Direct AMS C14	Direct	Exact Age	Unknown	Painting	N/A	(38)
M23, Calvert Ranges, Western Australia	-23.966667	122.966667	2'085	759	Australia	2010	Direct radiocarbon dating of pigment sampled	Direct	Exact age	Yes	Painting	N/A	(4)
Malangine Cave, Nene Valley, South Australia	-38.05	140.69	6'348	5'046	Australia	2010	Radiocarbon dating of speleothem deposit	Indirect	Minimum age	Yes	Figure Fluting & Engraving	No	(4)
Mámoa do Monte: Dos Marxos	42.648475	-7.946347	6'110	5'495	Portugal	2005	Direct AMS C14 of paint	Direct	Exact age	Yes	Painting	N/A	(5)
Marjar - East Alligator, Northern territory, Australia	-13.092293	132.393766	191	191	Australia	2010	Direct radiocarbon dating of beeswax sample from motif	Direct	Exact age	Yes	Beeswax	N/A	(4)
Mennge-ya 1, Northern Territory (near Willeroo)	-15.29028	131.575195	4'010	4'010	Australia	2010	Radiocarbon dating of base of the cortex	Indirect	Minimum age	No	Engraving	No	(4)
Messak Plateau, Fezzan, Libya	25.75	11.833333	6'080	5'150	Libya	2010	Radiocarbon dating on associated stone monuments	Indirect	N/A	No	Engraving	N/A	(39)
Mickey Springs 31, Hughenden, Queensland, Australia	-20.85	144.2	5'929	5'929	Australia	2010	Radiocarbon dating	Unknown	Unknown	Yes	Engraving	No	(4)
Moonface site, Queensland, Australia	-21.5097	140.6679	796	796	Australia	2010	Direct radiocarbon dating of charcoal sampled	Direct	Exact age	Yes	Painting	Yes	(4)
Moses Cave, Arnhem Land, Northern Territory, Australia	-12.430204	130.882379	274	274	Australia	2010	Direct radiocarbon from beeswax sample from motif	Direct	Exact age	Yes	Beeswax	No	(4)
Mount Manning, Western Australia	-30.12203	119.742604	586	182	Australia	2010	Indirect radiocarbon dating of charcoal ochre layers associated with drawings	Indirect	N/A	Yes	Drawing	No	(4)
Mungana Site, Queensland, Australia	-17.118416	144.398988	3'644	1'177	Australia	2010	Direct radiocarbon dating of charcoal sampled	Direct	Exact age	Yes	Drawing	No	(4)
Nangalor (Nanguluwur), Kakadu National Park, Northern Territory, Australia	-13.092293	132.393766	5'570	776	Australia	2010	Indirect radiocarbon dating of mineral salts from rock art surface sampled	Indirect	Minimum Age	Yes	Painting	No	(4)
Nara Inlet, Queensland	-20.15°	148.9	2'489	2'489	Australia	2010	Radiocarbon dating of charcoal sample	Unknown	Unknown	Yes	Unknown	N/A	(4)

Natal Drakkenberg, South Africa	-29.466667	29.266667	675	402	South Africa	1997	AMS Radiocarbon dating Andra 3 through associated plant fibers	Indirect	N/A	Yes	Painting	No	(40)
Nawarla Gabarnmang, Jawoyn Country, Arnhem Land Australia	-12.1685	133.8335	27630	27630	Australia	2013	Direct radiocarbon dating of charcoal pigment	Direct	Exact age	Yes	Painting	N/A	(41)
Nerja, Spain	36.785916	-3.804483	23'821	23'821	Spain	2013	Radiocarbon dating	Indirect	Minimum age	Yes	Drawings and torch rubbings	N/A	(26)
Ngarradj Warde Djobkeng, Northern Territory	-12.3	132.57	10'083	9'171	Australia	2010	Indirect radiocarbon dating of mineral salts from rock art surface sampled	Indirect	Minimum age	Yes	Painting	N/A	(4)
Ojo Guareña, Burgos, Spain	43.034337	-3.66452	11'540	10'950	Spain	2009	Direct radiocarbon dating of coal pigment	Direct	Exact age	Unknown	Paintings	Yes	(42)
Padahlin, Taunggyi District, Shan State, Myanmar	20.763697	96.920913	7'740	1'750	Myanmar	1971	AMS Radiocarbon dating	Indirect	Unknown	Unknown	Painting	Yes	(43)
Painted Shelter, Queensland, Australia	-16.1295	144.1289	2'420	2'420	Australia	2010	Direct radiocarbon	Direct	Exact Age	No	Painting	Yes	(4)
Panaramitee, Flinders Ranges, South Australia	-31.416667	138.75	43'140	3'575	Australia	2010	Indirect radiocarbon dating of rock varnish	Indirect	Minimum age	No	Engraving	No	(4)
Pech Merle, France	44.507308	1.64408	24'700	24'700	France	2001	Radiocarbon dating	Direct	Exact age	Unknown (Likely no	Painting	Yes	(13)
Pedra Cuberta	43.089554	-8.984605	5'775	5'620	Spain	2005	Radiocarbon AMS	Direct	Exact	Yes	Painting	Yes	(5)
Pedra da Moura, Vimianzo, A Coruña, Spain	43.081351	-8.977859	5'745	5'745	Spain	2005	Direct radiocarbon dating from megalithic paint	Direct	Exact age	Yes	Painting	N/A	(5)
Pedra Pintada, Monte Alegre, Brazil	-2.051761	54.182912	11'145	10'230	Brazil	1996	Radiocarbon dating (56) and thermoluminescence (13)	Indirect	Minimum age	No	Painting	Yes	(44)
Pete's Chase, Queensland	-16.1295	144.1289	2'090	310	Australia	2010	Direct radiocarbon dating of pigment sampled	Direct	Exact age	No	Painting	Yes	(4)
Pilbara, Western Australia, Australia	-21.883333	116.766667	3'700	2'600	Australia	2009	Radiocarbon dating	Indirect	Minimum age	Unknown	Petroglyphs	Yes	(45)
Pomongwe Cave, Zimbabwe	-20.547412°	28.513674	4'810	4'090	Zimbabwe	1983	Direct radiocarbon dating from spalls with paint from 2 layers	Direct	Exact age	Unknown	Painting	N/A	(6)
Pondra, Cantabria, Spain	43.266475	-3.423179	22'000	22'000	Spain	2013	Thermoluminescen	Indirect	Minimum age	Unknown	Painting	Yes	(46)
Possum Cave, Queensland, Australia	-10.7°	142.516667	9'501	2'217	Australia	2010	Radiocarbon dating on oxalate sampled	Indirect	Minimum age	Yes	Engraving	No	(4)
Prung-Cart Cave, South Australia (near Millicent)	-37.090413	140.829791	2'783	1'076	Australia	2010	Radiocarbon dating on calcite sampled	Indirect	Minimum age	Yes	Figure fluting	Unknown	(4)
Puritijarra, Cleland Hills, Northern Territory, Australia	-23.883333	130.866667	2'747	548	Australia	2010	Radiocarbon dating on oxalate sampled	Indirect	Minimum age	Yes	Engraving	No	(4)

Quinkans B6 Rockshelter, Queensland, Australia	-15.6286	144.5308	2'999	845	Australia	2010	Radiocarbon dating on oxalate sampled	Indirect	Minimum Age	Yes	Engraving & Painting	No	(4)
Qurta, Egypt	24.629167	32.9625	17'000	10'000	Egypt	2011	Direct Optically Stimulated Luminescence (OSL)	Direct	Exact Age	Unknown	Petroglyph	Yes	(47)
Racecourse Site, Queensland, Australia	-17.1747	144.4994	2'031	2'031	Australia	2010	Direct radiocarbon dating on charcoal pigment	Direct	Exact Age	Yes	Drawing	No	(4)
Red Lady, Queensland, Australia	-15.762116	144.257562	8'213	8'213	Australia	2010	Indirect radiocarbon dating on silica sampled	Indirect	Minimum Age	Yes	Painting	Yes	(4)
Robin Hood Cave and Church Hole, Creswell Crags, UK	53.263491	-1.193529	15'700	13'200	UK	2005	Uranium-series disequilibrium dating on thin layer of flowstones covering the surface (Minimum age)	Indirect	Minimum Age	Yes	Engravings	Yes	(48)
RSA TYN2 , Drakensberg Mountains, Eastern Cape, South Africa	-29.466667	29.266667	2'009	1'971	South Africa	2011	Direct radiocarbon dating	Direct	Exact age	Yes	Paintings	Unknown	(49)
Sandy Creek 1 & 2, Queensland, Australia	-16	144	29'440	2'964	Australia	2005	Indirect radiocarbon dating on oxalate sampled	Indirect	Minimum Age	Yes	Painting	Yes	(50)
Serpent's Glen 1, Wiluna, Western Australia	-25.216667	120.75	3'417	377	Australia	2010	Direct radiocarbon dating on paint sampled	Direct	Exact Age	Yes	Painting	No	(4)
Serra de Capivara, Brazil	-8.695278	-42.586267	9'863	1'028	Brazil	2013	Radiocarbon dating	Indirect	N/A	Yes	Paintings	N/A	(51)
Snake Site, Cannon Hill, Northern Territory, Australia	-12.3	132.57	563	563	Australia	2010	Indirect radiocarbon dating on mineral salts from rock art surface	Indirect	Minimum age	Yes	Painting	N/A	(4)
Spirit Cave, Anbangbang, Kakadu, Northern Territory, Australia	-12.865524	132.814001	14'182	3'747	Australia	2010	Indirect radiocarbon dating on oxalate sampled	Indirect	Minimum Age	Yes	Painting	No	(4)
Split rock, Queensland, Australia	-15.6525	144.4975	7'433	7'433	Australia	2010	Direct radiocarbon dating on silica sampled	Direct	Exact Age	Yes	Painting	N/A	(4)
Steenbokfontein Cave, South Africa	-32.161667	18.333333	8'370	2'200	South Africa	1999	AMS dating	Indirect	Minimum age	No	Painting	No	(52)
Sturt Meadows, New South Wales, Australia	-31.11	140.4	12'237	11'978	Australia	2010	Indirect radiocarbon dating on calcium carbonate sampled	Indirect	Minimum Age	Yes	Engraving	N/A	(4)

Sulawesi, Indonesia	-1.8479	120.5279	44'000	17'770	Indonesia	2014	Uranium-series dating of coralloid speleothems	Indirect	Minimum age	Yes	Hand stencils and paintings	Yes	(53)
Tassili-n-Ajjer, Algeria	25.813595	8.133856	8'237	2'287	Algeria	2012	AMS Radiocarbon dating	Indirect	N/A	Yes	Paintings	Yes	(54)
Tennessee, Cumberland Plateau	35.949603	-85.027047	5'698	N/A	USA	2013	AMS Radiocarbon dating	Direct	Exact Age	Yes	Charcoal pictograph	Yes	(55)
Tito Bustillo Cave, Spain	43.460706	-5.067392	36'200	29'650	Spain	2012	U-series disequilibrium dating	Indirect	Mixed	Yes	Paintings	Yes	(14)
uKhalamba, South Africa	-29.380485	29.546	4'050	990	South Africa	2003	Indirect radiocarbor	Indirect	Maximum age	Yes	Painting	Yes	(8)
Unnamed sites 1-3, Kimberley, Western Australia	-17.34918	125.915207	23'800	Modern	Australia	2010	Indirect radiocarbon dating from sampled mud-wasp nest overlying paintings	Indirect	Minimum Age	No	Painting	Yes	(4)
Urdiales, Spain	43.368822	-3.215635	15'223	15'223	Spain	2013	Radiocarbon dating	Direct	Exact age	Yes	Painting	Yes	(26)
Urkan-e-Rub, Lower Jordan Valley, Israel	32.422877	35.302723	16'750	16'750	Israel	2010	Unknown	Unknown	Unknown	Unknown	Engraving	No	(56)
Villars, France	45.442277	0.785135	21'735	17'473	France	2013	Radiocarbon dating	Direct	Exact age	Yes	Drawings and torch rubbings	No	(26)
Walkunder Arch Cave, Queensland, Australia	-17.2297	144.5169	34'254	3'575	Australia	2010	Indirect radiocarbon dating on oxalate, graphite sampled	Indirect	Maximum age for date to use; different samples have minimum age, maximum age, middle date, and supporting date	Yes	Paintings & Engraving	N/A	(4)
Wanga East, Northern Territory, Australia	-24.19	131.4	8'093	1'332	Australia	2010	Indirect radiocarbon dating on oxalate formation	Indirect	Minimum age	Yes	Engraving	Yes	(4)
Waterfall Cave, New South Wales, Australia	-35.42	150.11	604	N/A	Australia	2010	Direct radiocarbon dating on carbon particles within relict areas of pgiment	Direct	Exact Age	Yes	Painting	No	(4)
Wharton Hill, Australia	-32.64	139.77	36'400	36'400	Australia	1992	Radiocarbon dating	Indirect	Minimum age	No	Petroglyph	Yes	(57)
Winnemucca Lake, Nevada, Usa	40.12185	-119.339623	12'500	12'500	USA	2013	Radiocarbon dating	Indirect	Minimum age	Yes	Painting	No	(58)
Wonderwerk Cave, South Africa	-27.84673	23.55418	10'200	1'210	South Africa	1981	Radicarbon dating (minimum age)	Indirect	Minimum age	Unknown	Engraving	No	(59)
Wurik (Mann River E1002, 1004, 1005)., Northern Territory, Australia/Yikarrakkal (Mann River A1005), Northern Territory, Australia	-12.219481	134.143519	646	183	Australia	2010	Direct radiocarbon	Direct	Exact Age	Beeswax	Beeswax	Yes	(4)

Yam Camp, Cape York, Queensland, Australia	-15.7823	144.2341	682	602	Australia	2010	Direct radiocarbon dating from plant fibre binders (Earliest age) & indirect radiocarbon dating with oxalate sample (Latest age)	Direct	Exact Age, but latest date is minimum age	Yes	Painting	Yes	(4)
Yiwarlarlay, Northern Territory, Australia	-12.36686	130.88125	4'592	3'386	Australia	2010	Indirect radiocarbor	Indirect	Minimum age	Yes	Engraving	Yes	(4)
Yunta Springs, South Australia	-32.54	139.55	17'020	1'398	Australia	2010	Indirect radiocarbor	Indirect	Minimum age	Yes	Engraving	Mixed	(4)

Note: A CSV version of this table is available as a separate file

References for SI Table 1

1. White R, Mensan R, Bourrillon R, Cretin C, Higham TF, Clark AE, et al. Context and dating of Aurignacian vulvar representations from Abri Castanet, France. Proc Natl Acad Sci. 2012;109: 8450–8455.
2. García-Diez M, Hoffmann DL, Zilhão J, de las Heras C, Lasheras JA, Montes R, et al. Uranium series dating reveals a long sequence of rock art at Altamira Cave (Santillana del Mar, Cantabria). J Archaeol Sci. 2013;40: 4098–4106.
3. González-Sainz C, Ruiz-Redondo A, Garate-Maidagan D, Iriarte-Avilés E. Not only Chauvet: dating Aurignacian rock art in Altxerri B Cave (northern Spain). J Hum Evol. 2013;65: 457–464.
4. Langley MC, Taçon PSC. The age of Australian rock art: A review. Aust Archaeol. 2010;71: 70–73. doi:10.1080/03122417.2010.11689386
5. Steelman KL, Ramírez FC, Valcarce RF, Guilderson T, Rowe MW. Direct radiocarbon dating of megalithic paints from north-west Iberia. Antiquity. 2005;79: 379–389.
6. Thackeray AI. Dating the rock art of southern Africa. Goodwin Ser. 1983;4: 21–26. doi:10.2307/3858098
7. Bednarik RG, Kumar G, Watchman A, Roberts RG. Preliminary results of the EIP Project. 2005. Available: http://ro.uow.edu.au/scipapers/3611/
8. Mazel AD, Watchman AL. Dating rock paintings in the uKhahlamba-Drakensberg and the Biggarsberg, KwaZulu-Natal, South Africa. South Afr Humanit. 2003;15: 59–73.
9. Francis JE, Loendorf LL, Dorn RI. AMS radiocarbon and cation-ratio dating of rock art in the Bighorn Basin of Wyoming and Montana. Am Antiq. 1993;58: 711–737.
10. Taçon PS, Boivin N, Petraglia M, Blinkhorn J, Chivas A, Roberts RG, et al. Mid-Holocene age obtained for nested diamond pattern petroglyph in the Billasurgam Cave complex, Kurnool District, southern India. J Archaeol Sci. 2013;40: 1787–1796.
11. Watchman A, Cole N. Accelerator radiocarbon dating of plant-fibre binders in rock paintings from northeastern Australia. Antiquity. 1993;67: 355–358. doi:10.1017/S0003598X00045415
12. Bendrey R. Review of Wadi Sura–The Cave of Beasts edited by Rudolph Kuper. Pastoralism. 2014;4: 2. doi:10.1186/2041-7136-4-2
13. Valladas H, Clottes J, Geneste J-M, Garcia MA, Arnold M, Cachier H, et al. Palaeolithic paintings: Evolution of prehistoric cave art. Nat Lond. 2001;413: 479. doi:http://dx.doi.org/10.1038/35097160
14. Pike AWG, Hoffmann DL, García-Diez M, Pettitt PB, Alcolea J, Balbín RD, et al. U-series dating of paleolithic art in 11 caves in Spain. Science. 2012;336: 1409–1413. doi:10.1126/science.1219957
15. Valladas H, Cachier H, al et. Direct radiocarbon dates for prehistoric paintings at the Altamira, El Castillo and Niaux caves. Nat Lond. 1992;357: 68.
16. Valladas H, Tisnérat-Laborde N, Cachier H, Arnold M, Quirós FB de, Cabrera-Valdés V, et al. Radiocarbon AMS Dates for paleolithic cave paintings. Radiocarbon. 2001;43: 977–986. doi:10.1017/S0033822200041643
17. Butzer KW, Fock GJ, Scott L, Stuckenrath R. Dating and context of rock engravings in southern Africa. Science. 1979;203: 1201–1214.
18. Zorich Z. From the Trenches - Drawing Paleolithic Romania - Archaeology Magazine Archive. [cited 20 Jul 2017]. Available: http://archive.archaeology.org/1201/trenches/coliboaia_cave_romania_charcoal_drawings.html
19. Huyge D, Watchman A, De Dapper M, Marchi E. Dating Egypt's oldest 'art': AMS 14C age determinations of rock varnishes covering petroglyphs at El-Hosh (Upper Egypt). Antiquity. 2001;75: 68–72.
20. Mercier N, Valladas H, Aubry T, Zilhão J, Jorons JL, Reyss J-L, et al. Fariseu: first confirmed open-air palaeolithic parietal art site in the Côa Valley (Portugal). Antiquity. 2006;80. Available: http://www.antiquity.ac.uk/projgall/mercier/
21. Sand C, Valladas H, Cachier H, Tisnérat-Laborde N, Arnold M, Bolé J, et al. Oceanic rock art: first direct dating of prehistoric stencils and paintings from New Caledonia (Southern Melanesia). Antiquity. 2006;80: 523–529.
22. Watchman A. A review of the theory and assumptions in the AMS dating of the Foz Côa petroglyphs, Portugal. Rock Art Res. 1996;13: 21–29.
23. Moure Romanillo A, Gonzalez Morales M. Datation 14C d'une zone décorée de la grotte Fuente del Salin. Int Newsl Rock Art - INORA. 1992.
24. Clottes J, Valladas H, Cachier H, Arnold M. Des dates pour Niaux et Gargas. Bull Société Préhistorique Fr. 1992;89: 270–274. doi:10.3406/bspf.1992.9532
25. Geib PR, Fairley HC. Radiocarbon Dating of Fremont Anthropomorphic Rock Art in Glen Canyon, South-central Utah. J Field Archaeol. 1992;19: 155–168. doi:10.1179/009346992791548932

26. Valladas H, Kaltnecker E, Quiles A, Tisnérat-Laborde N, Genty D, Arnold M, et al. Dating French and Spanish prehistoric decorated caves in their archaeological contexts. Radiocarbon. 2013;55: 1422–1431. doi:10.1017/S0033822200048359
27. Broglio A, De Stefani M, Gurioli F, Pallecchi P, Giachi G, Higham T, et al. L'art aurignacien dans la décoration de la Grotte de Fumane. L'Anthropologie. 2009;113: 753–761. doi:10.1016/j.anthro.2009.09.016
28. Ambert P, Guendon J-L, Galant P, Quinif Y, Gruneisen A, Colomer A, et al. Attribution des gravures paléolithiques de la grotte d'Aldène (Cesseras, Hérault) à l'Aurignacien par la datation des remplissages géologiques. /data/revues/16310683/00040003/04001691/. [cited 25 Jul 2017]. Available: http://www.em-consulte.com/en/article/30133
29. Jaubert J, Genty D, Valladas H, Camus H, Courtaud P, Ferrier C, et al. The chronology of human and animal presence in the decorated and sepulchral cave of Cussac (France). Quat Int. 2017;432: 5–24. doi:10.1016/j.quaint.2016.01.052
30. Plagnes V, Causse C, Fontugne M, Valladas H, Chazine J-M, Fage L-H. Cross dating (Th/U-14 C) of calcite covering prehistoric paintings in Borneo. Quat Res. 2003;60: 172–179.
31. Nelson DE, Chaloupka G, Chippindale C, Alderson MS, Southon JR. Radiocarbon dates for beeswax figures in the prehistoric rock art of Northern Australia. Archaeometry. 1995;37: 151–156. doi:10.1111/j.1475-4754.1995.tb00733.x
32. Steelman KL, Rowe MW, Shirokov VN, Southon JR. Radiocarbon dates for pictographs in Ignatievskaya Cave, Russia: Holocene age for supposed Pleistocene fauna. Antiquity. 2002;76: 341–348. doi:10.1017/S0003598X00090426
33. Taçon PS, Aubert M, Gang L, Decong Y, Hong L, May SK, et al. Uranium-series age estimates for rock art in southwest China. J Archaeol Sci. 2012;39: 492–499.
34. Stasack E, Dorn RI, Lee G. First direct 14C ages on Hawaiian petroglyphs. Asian Perspect. 1996;35: 51–72.
35. Shchelinsky VE. Some results of new investigations at the Kapova Cave in the southern Urals. Proc Prehist Soc. 1989;55: 181–191. doi:10.1017/S0079497X00005387
36. Neves WA, Araujo AGM, Bernardo DV, Kipnis R, Feathers JK. Rock art at the pleistocene/holocene boundary in eastern South America. Petraglia MD, editor. PLoS ONE. 2012;7: e32228. doi:10.1371/journal.pone.0032228
37. O'Connor S, Aplin K, Pierre ES, Feng Y. Faces of the ancestors revealed: discovery and dating of a Pleistocene-age petroglyph in Lene Hara Cave, East Timor. Antiquity. 2010;84: 649–665. doi:10.1017/S0003598X00100146
38. Russ J, Hyman M, Rowe M. Direct radiocarbon dating of rock art. Radiocarbon. 1992;34: 867–872.
39. di Lernia S, Gallinaro M. The date and context of neolithic rock art in the Sahara: engravings and ceremonial monuments from Messak Settafet (south-west Libya). Antiquity. 2010;84: 954–975.
40. Mazel AD, Watchman AL. Accelerator radiocarbon dating of Natal Drakensberg paintings: results and implications. Antiquity. 1997;71: 445–449.
41. David B, Barker B, Petchey F, Delannoy J-J, Geneste J-M, Rowe C, et al. A 28,000 year old excavated painted rock from Nawarla Gabarnmang, northern Australia. J Archaeol Sci. 2013;40: 2493–2501. doi:10.1016/j.jas.2012.08.015
42. Corchón Rodríguez MS, Valladas H, Bécares Pérez J, Arnold M, Tisnerat N, Cachier H. Datación de las pinturas y revisión del Arte Paleolítico de Cueva Palomera (Ojo Guareña, Burgos, España). 2009. Available: https://gredos.usal.es/jspui/handle/10366/70469
43. Thaw UA. The "neolithic" culture of the Padah-lin Caves. Asian Perspect. 1971;14: 123–133.
44. Roosevelt AC, Lima da Costa M, Lopes Machado C, Michab M, Mercier N, Valladas H, et al. Paleoindian cave dwellers in the Amazon: the peopling of the Americas. Sci-N Y THEN Wash-. 1996; 373–384.
45. Mulvaney K. Dating the Dreaming: extinct fauna in the petroglyphs of the Pilbara region, Western Australia. Archaeol Ocean. 2009;44: 40–48.
46. Sauvet G. À la recherche du temps perdu. Méthodes de datations en art préhistorique. Available: https://www.researchgate.net/profile/Georges_Sauvet2/publication/289376793_A_la_recherche_du_temps_perdu_methodes_de_datations_en_art_prehistorique_L'exemple_des_sites_aurignaciens/links/568c0e1f08ae197e42689524.pdf
47. Huyge D, Vandenberghe DA, De Dapper M, Mees F, Claes W, Darnell JC. First evidence of Pleistocene rock art in North Africa: securing the age of the Qurta petroglyphs (Egypt) through OSL dating. Antiquity. 2011;85: 1184–1193.
48. Pike AWG, Gilmour M, Pettitt P, Jacobi R, Ripoll S, Bahn P, et al. Verification of the age of the Palaeolithic cave art at Creswell Crags, UK. J Archaeol Sci. 32: 1649–1655.
49. Bonneau A, Brock F, Higham T, Pearce DG, Pollard AM. An improved pretreatment protocol for radiocarbon dating black pigments in San rock art. Radiocarbon. 2011;53: 419–428.

50. Cole N, Watchman A. AMS dating of rock art in the Laura Region, Cape York Peninsula, Australia–protocols and results of recent research. Antiquity. 2005;79: 661–678.
51. Fontugne M, Shao Q, Frank N, Thil F, Guidon N, Boeda E. Cross-Dating (Th/U-14 C) of Calcite Covering Prehistoric Paintings at Serra da Capivara National Park, Piaui, Brazil. Radiocarbon. 2013;55: 1191–1198.
52. Jerardino A, Swanepoel N. Painted Slabs from Steenbokfontein Cave: The Oldest Known Parietal Art in Southern Africa. Curr Anthropol. 1999;40: 542–547. doi:10.1086/200051
53. Aubert M, Brumm A, Ramli M, Sutikna T, Saptomo EW, Hakim B, et al. Pleistocene cave art from Sulawesi, Indonesia. Nature. 2014;514: 223.
54. Hachid M, Le Quellec J-L, Amara A, Beck L, Heddouche A, Kaltnecker E, et al. Quelques résultats du projet de datation directe et indirecte de l'art rupestre saharien. Signs Which Times. 2012; 71–96.
55. Simek JF, Cressler A, Herrmann NP, Sherwood SC. Sacred landscapes of the south-eastern USA: prehistoric rock and cave art in Tennessee. Antiquity. 2013;87: 430–446.
56. Bednarik RG. An overview of Asian palaeoart of the Pleistocene. Proceedings of the IFRAO Congress. 2010. Available: http://www.ifrao.com/wp-content/uploads/2015/08/12Asia2.pdf
57. Dorn RI, Clarkson PB, Nobbs MF, Loendorf LL, Whitley DS. New Approach to the Radiocarbon Dating of Rock Varnish, with Examples from Drylands. Ann Assoc Am Geogr. 1992;82: 136–151.
58. Benson LV, Hattori EM, Southon J, Aleck B. Dating North America's oldest petroglyphs, Winnemucca Lake subbasin, Nevada. J Archaeol Sci. 2013;40: 4466–4476.
59. Thackeray AI, Thackeray JF, Beaumont PB, Vogel JC. Dated rock engravings from Wonderwerk Cave, South Africa. Science. 1981;214: 64–67. doi:10.1126/science.214.4516.64